



A novel method for resonant inelastic soft X-ray scattering *via* photoelectron spectroscopy detection

Georgi L. Dakovski,^{a*} Ming-Fu Lin,^a Daniel S. Damiani,^a William F. Schlotter,^a Joshua J. Turner,^a Dennis Nordlund^b and Hirohito Ogasawara^b

^aLinac Coherent Light Source, SLAC National Accelerator Laboratory, 2575 Sand Hill Road, Menlo Park, CA 94025, USA, and ^bStanford Synchrotron Radiation Lightsource, SLAC National Accelerator Laboratory, 2575 Sand Hill Road, Menlo Park, CA 94025, USA. *Correspondence e-mail: dakovski@slac.stanford.edu

Received 7 April 2017

Accepted 15 August 2017

Edited by S. Svensson, Uppsala University, Sweden

Keywords: RIXS; soft X-ray; spectroscopy; FEL.

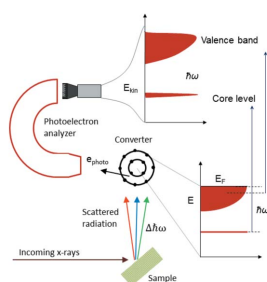
A method for measuring resonant inelastic X-ray scattering based on the conversion of X-ray photons into photoelectrons is presented. The setup is compact, relies on commercially available detectors, and offers significant flexibility. This method is demonstrated at the Linac Coherent Light Source with ~ 0.5 eV resolution at the cobalt L_3 -edge, with signal rates comparable with traditional grating spectrometers.

1. Concept

Inelastically scattered X-rays often provide valuable information about the electronic structure of materials. When the X-rays are tuned to a particular absorption edge of a given atom, the resonant excitation of the core hole provides element specificity. Simultaneously, the emitted X-ray energy-loss spectrum can probe charge-neutral excitations such as electron–hole pairs, magnons and phonons on this local core hole site. Resonant inelastic X-ray scattering (RIXS) (Nordgren & Rubensson, 2013) has grown to become a mature technique, especially for studies of correlated electron materials (Ament *et al.*, 2011), gases (Hennies *et al.*, 2010) and liquids (Wernet *et al.*, 2015). In RIXS, the absorption and emission of light are treated as a coherent process leaving the system in a state where the core hole is filled. Therefore, the energy resolution is not limited by the short lifetime of the core hole as is the case for traditional non-resonant photoionization.

RIXS is not constrained to a specific energy range. Historically, the importance of 3d transition metal oxides and the ability to access the 3d frontier orbitals directly from the 2p core hole *via* the dipole transition has placed an emphasis on using X-rays below 1 keV. The most widely used detection scheme for soft X-ray RIXS involves dispersing the scattered photons by wavelength *via* a grating and recording the spectra with a two-dimensional position-sensitive detector (Nordgren & Guo, 2000). Significant improvements in the manufacturing of high-quality gratings, together with the development of high-brilliance synchrotrons, have enabled soft X-ray emission spectrometers with remarkable resolving power (Ghiringhelli *et al.*, 2006), providing a significant enhancement of RIXS capabilities.

Several challenges, however, remain that limit the scientific applicability of RIXS in solids: the inherently low fluorescence yield in the soft X-ray range, the need for very small X-ray spot sizes in the dispersing direction (in a slit-less design), the limited angular acceptance, and the need for expensive



infrastructure such as high-quality gratings and high-spatial-resolution two-dimensional detectors (Soman *et al.*, 2013).

Some recent developments offer potential solutions to a subset of these issues. For example, high-intensity X-ray pulses from free-electron lasers (FELs) can enable stimulated inelastic scattering, but overcoming the low fluorescence yield limitation remains to be demonstrated (Beye *et al.*, 2013). Furthermore, an emerging technology for X-ray spectroscopy, transition edge sensors (TES) (Irwin & Hilton, 2005), recently achieved sub-eV resolution. Because thermal detection is used in TES, it does not rely on geometrical dispersion, indicating that large acceptance angles and spot sizes on the sample are possible (Uhlir *et al.*, 2015). However, the TES technology does not have a short-term path towards sub- ~ 0.5 eV resolution in the soft X-ray range and the applicability for high-resolution RIXS is therefore limited. Thus, there is significant interest in exploring alternative methods and schemes for detecting inelastically scattered soft X-ray photons more efficiently, preferably providing a path towards both high-resolution and high-throughput measurements.

Here, we present a novel method that combines several favorable characteristics over traditional soft X-ray detection technologies. Among the noteworthy advantages are: large spot size capability, compact design with reduced sensitivity to geometrical aberrations, vibrations and thermal instabilities, together with a dependence on commercially available instrumentation. The ability to avoid the need for tight X-ray focusing is especially important for beam-damage-sensitive samples. The compact design and availability of commercially available detection is a significant departure from the current trend of developing large-scale RIXS spectrometers.

This method takes advantage of the photoelectron as a carrier of energetic information, as schematically shown in Fig. 1. When irradiated with monochromatic X-ray photons, photoelectrons carry information about the final state left behind, from which electronic structural information of the system is attainable. This concept, however, can be inverted: for a material with a well defined spectral response and sufficiently sharp features, the photoelectron can also be used to carry information about an unknown source of X-rays. This idea was originally put forward by M. O. Krause and named ‘photoelectron spectrometry for analysis of X-rays’ (PAX) (Krause, 1965), more than 50 years ago. At the time, noble gases were used as converter atoms, taking advantage of naturally sharp absorption peaks. The investigated soft X-ray sources were the emission spectra of atomic species typically covering hundreds of electron-volts.

In this study we make use of the conceptual ability of PAX and apply it to RIXS, where the typical range of the inelastically scattered X-rays is on the order of 10 eV. A sharp well known feature in the monochromatic photoexcitation of a converter atom, that can be either a gas or a solid, could be used to encode the spectrum of inelastically scattered X-rays into a spectrum of photoelectrons. This spectrum is collected by an electron energy analyzer. The resultant photoelectron spectrum is a convolution of the unknown inelastic X-ray spectrum with the response of the converter atom to a

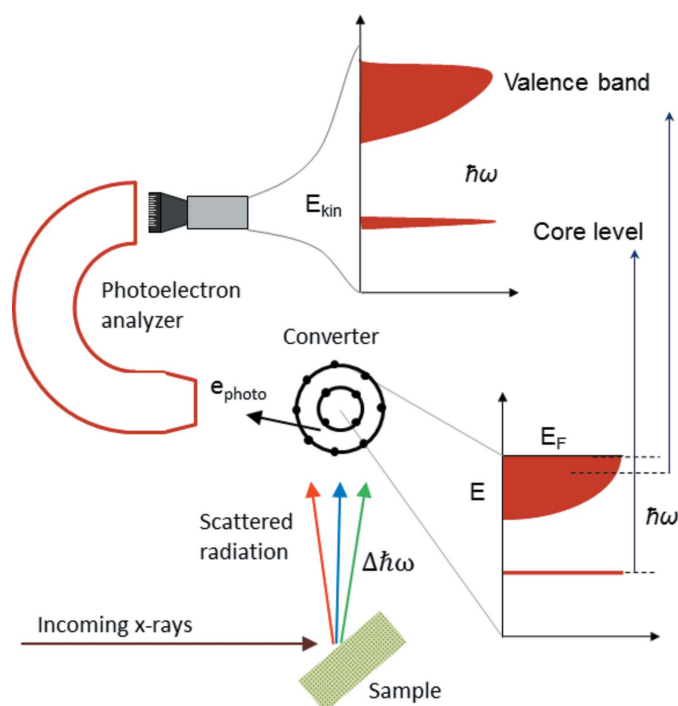


Figure 1 Schematic of the PAX concept. The emitted X-rays are converted into photoelectrons from a target with a well defined monochromatic spectral response (either a gas or solid). The convolved photoelectron response is resolved with an electron analyzer.

monochromatic X-ray beam. In fact, a typical photoemission spectrum is an extreme case of this, where the measured photoelectron spectrum is a convolution of the incoming X-ray profile (typically a Gaussian) and the natural response function of the sample. If the natural width of the spectral feature and the intrinsic resolution of the electrostatic analyzer is small enough, the original RIXS spectrum can then be retrieved by the process of deconvolution (Ebel, 1975).

The main benefits of PAX can be easily recognized. Unlike grating spectrometers, PAX does not work as an imaging spectrometer that relies on geometrical dispersion, where the resolution is hinged upon a limited entrance slit or, similarly, a small X-ray spot on the sample. In PAX, the X-ray spot size is not constrained and, in fact, if the beam is significantly defocused, more photons can be used before beam damage or non-linear effects set in. While concerns about non-linear effects are not an issue at third-generation storage ring light sources in general, it is especially important for RIXS at FELs. Additionally, the entire system, consisting of the sample, converter atom and detector, can be placed in a single ultra-high-vacuum chamber. A suitable mechanism for rotating the detector sub-system would allow for momentum-resolved studies. Furthermore, controlling the angular acceptance of the converter atom with respect to the scattered X-rays would allow a trade-off between collected signal and angular resolution. Moreover, instrumentation for energy-resolving photoelectrons, rather than photons, has benefited from a larger market and associated industrial optimization. Current state-of-the-art hemispherical analyzers collect a significant

fraction of the photoemitted electrons, and the use of retarding electrostatic lenses gives the option of detecting photoelectrons with adjustable and potentially high energy resolution (Mårtensson *et al.*, 1994). For the PAX concept, if very high resolution is desired and the beamline can provide sufficiently narrow-band pulses, one can use the Fermi edge as a sharp feature to encode the inelastic X-ray spectrum. Lastly, PAX is not limited to the soft X-ray range, and could be extended to tender and hard X-rays without changing detection technology, and without the restriction of using only particular Bragg crystal reflections.

2. Experimental setup

We have carried out a demonstration experiment on the SXR Instrument at the Linac Coherent Light Source (LCLS) (Schlotter *et al.*, 2012; Dakovski *et al.*, 2015) with the objective to test the validity of the concept using a suitable converter atom, estimate signal levels, and compare these with typical grating-based spectrometers. We selected the RIXS spectrum from CoO, a well known system that displays pronounced $d-d$ excitations when the incident photon energy is scanned across the absorption spectrum (Chiuzbăian *et al.*, 2008; van Schooneveld *et al.*, 2012). Measurements were completed on a single-crystal at (100) orientation mounted at 20° incident grazing angle, at room temperature. The scattering geometry was vertical, with σ -polarized X-rays, *i.e.* polarized perpendicularly to the scattering plane (horizontal in the laboratory reference plane).

The X-ray photons emitted from the sample were incident on a gold foil (Sigma Aldrich), 100 nm-thick, approximately 10 mm \times 10 mm wide, located about 20 mm away from the CoO sample. A 200 nm thin Al foil (Luxel) was placed between the sample and the gold to prevent Auger and secondary electrons emitted by the CoO sample from interfering with the measured photoelectrons. The choice of gold as a converter atom was made based on the fact that typical experiments at SXR require monochromatic X-rays and use the beamline monochromator providing a resolving power of ~ 3000 (Heimann *et al.*, 2011). Therefore, the well known sharp $4f$ peaks of gold, at binding energies of 84 eV and 87.6 eV, can be used to reconstruct the unknown inelastic spectrum. It should be noted that, if very high energy resolution is desired, one can shift to using the Fermi edge portion of the spectrum, where, upon cooling, one can expect excellent resolution. For this experiment no cooling was employed.

Photoelectrons were recorded using a VG Scienta R3000 hemispherical electron analyzer, which was operated exclusively using the 0.4 mm entrance slit, and with a pass energy of 200 eV, which resulted in an analyzer resolution of 295 meV. All measurements were recorded in the so-called imaging (transmission) mode. The two-dimensional images from the Scienta detector (consisting of a double microchannel plate stack plus phosphor screen) were recorded using a CCD camera (Adimec-OPAL) capable of reading out full images at the repetition rate of the FEL, 120 Hz. Due to the low detection count rates and the camera fast readout capabilities,

single photon events were isolated by appropriate thresholding and the resultant images were summed along the non-dispersive direction to produce one-dimensional spectra.

While in principle this experiment could have been carried out at a synchrotron source, testing the concept at a FEL was motivated by the following two reasons: first, with the prospect of a three to four order increase in X-ray flux, we wanted to perform benchmarking with the current capabilities at LCLS, which will allow us to project future performance with a good level of confidence; secondly, photoemission at a FEL is typically accompanied by the space charge effect if the beam is not attenuated below certain threshold levels (Dell'Angela *et al.*, 2015). Even though PAX does not use the direct FEL beam, it still relies on the process of photoemission, and, hence, energy resolution degradation is possible. Therefore, we wanted to investigate whether this would cause an issue using typical FEL single-pulse characteristics.

3. Gold characterization

As a first step, we placed the gold film directly in the X-ray beam and collected the reference photoemission spectrum of the $4f$ resonances. We used soft X-rays resonant with the Co L_3 edge at 778 eV with a bandwidth of 260 meV, limited by the beamline monochromator. In addition, the X-rays were focused to about a 300 μm \times 900 μm spot size. With the Au foil placed at 5° relative to the incoming beam, the effective spot on the sample was 3500 μm \times 900 μm . The results are shown in Fig. 2. We recorded spectra at different intensity levels to ensure that no distortion of the spectra (whether from a shift and/or broadening) is present due to the space-charge effect. The data shown were accumulated in approxi-

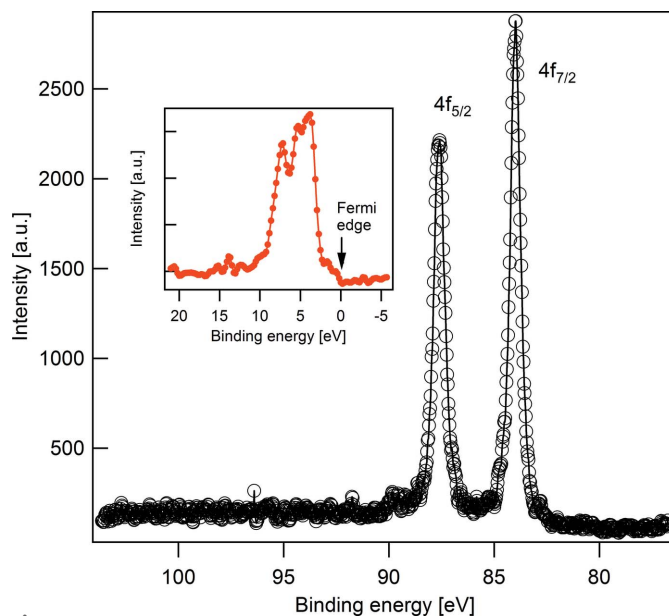


Figure 2 $4f$ peaks in Au. Inset: valence band spectrum. The sharp $4f$ resonances represent the response function of the converter-analyzer system and are used to encode the spectrum of the inelastically scattered X-rays. If very high resolution is desired, the region in the vicinity of the Fermi edge could be used instead.

mately 45 min, once the X-rays were attenuated to about 10^5 photons pulse⁻¹ (0.3 nJ cm^{-2}), which was deemed acceptable since it resulted in a distortion-free spectrum. A Gaussian fit to the $4f$ peak at 84 eV revealed a FWHM of 550 meV, which agrees well with the vectorial contribution from the incident bandwidth spread, the analyzer resolution and the intrinsic width ($\sim 200 \text{ meV}$) of the peak (Takata *et al.*, 2005).

For reference we also collected a spectrum of the valence states of Au, shown in the inset of Fig. 2, over a period of 30 min. The spectrum agrees well with other measurements using high-energy X-rays (Takata *et al.*, 2005). The signal intensity from electrons in the vicinity of the Fermi edge is weaker by a factor of ~ 150 from the signal from the $4f$ peaks due to the reduced photoionization cross section. Therefore we plan to pursue PAX from the valence states in Au in the near future with an improved version of the current setup.

4. Spectra from CoO

With the reference photoelectron spectrum of Au accurately characterized, we placed the X-ray beam directly on the sample of interest, CoO. The incoming pulse energy of individual FEL pulses was $\sim 2 \text{ mJ}$. After transmission of all the beamline optics, diffraction from the grating monochromator and spectrally selecting a bandwidth of 260 meV, $\sim 2 \mu\text{J}$ pulses were incident on the sample (Tiedtke *et al.*, 2014). Due to the small-incident-angle geometry, the effective X-ray spot size on the sample was $900 \mu\text{m} \times 900 \mu\text{m}$, resulting in an X-ray fluence of 0.25 mJ cm^{-2} , well within the regime of linear X-ray–matter interaction (Beye *et al.*, 2013). We made nine measurements, changing the incident photon energy each time by $\sim 1 \text{ eV}$ across the L_3 resonance of Co to construct the RIXS map of inelastic energy loss *versus* incident energy. Two representative spectra, one below and one above the main absorption peak, are shown in Fig. 3. The data are shown as black dots, where the x -axis represents the photoelectron energy, and the y -axis is proportional to the accumulated number of counts over the course of a 30 min measurement. The only data processing employed was to bin the spectra in the dispersion direction into 200 meV bins for improved signal quality. On average, we obtain very similar count rates between the RIXS spectrum measured using the $4f$ peaks in Au with the PAX technique and that of the direct measurement with a heavily attenuated beam. This result was to be expected: when calibrating the $4f$ peaks with the direct beam, we attenuated by a factor of $\sim 10^{-5}$. When the unattenuated beam was placed on CoO, we expected that from the fluorescence yield ($\sim 10^{-3}$) and the angular acceptance ($\sim 10^{-2}$) we would reach a similar flux of scattered X-rays. This indicates that space charge is not an issue for the PAX method. Moreover, using a simple formula for estimating the space charge effect (Long *et al.*, 1996) indicates that at $\sim 10^5$ photons pulse⁻¹ the kinetic energy of the photoelectrons is modified only by $\sim 10 \text{ meV}$ which is beyond the sensitivity of the current experiment.

When the incident photon energy is below the Co resonance, it is observed that the photoelectron spectrum is

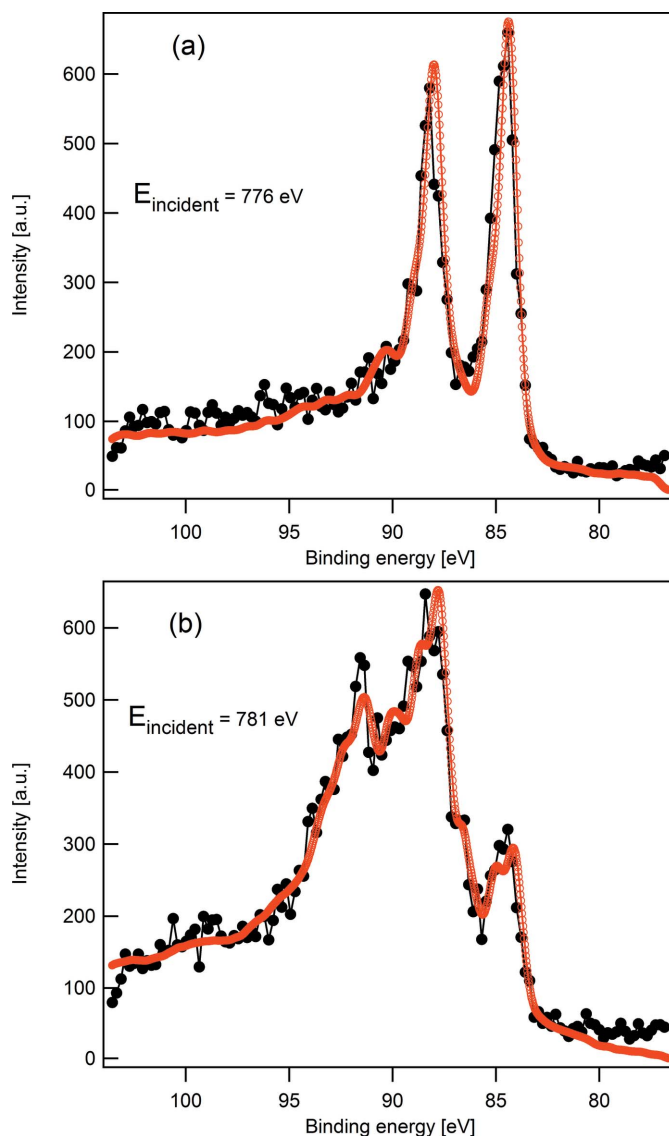


Figure 3 Photoelectron spectra (a) below and (b) above the Co L_3 resonance. The black dots represent the data, while the red curves are fits generated with an iterative, non-linear, least-squares fitting procedure. This process takes into account the convolution of the simulated RIXS spectrum (see §5) with the instrument response function, Fig. 2.

qualitatively very similar to the reference spectrum of the $4f$ peaks shown in Fig. 2. Note that this is apart from some obvious broadening of the peaks and the appearance of additional spectral weight at the energy-loss side. This hints that the RIXS spectrum is dominated by one spectral feature, the quasi-elastic line. As the incident photon energy is increased, the recorded spectrum begins to look considerably more complex, signifying that the RIXS spectrum becomes more heavily modulated.

5. Data retrieval

As mentioned earlier, the procedure for extracting the unknown RIXS spectrum involves the deconvolution of the

measured $4f$ spectrum, playing the role of a point-spread function, from the recorded photoelectron spectrum. While conceptually simple, this procedure is non-trivial in practice. For the purposes of our demonstration experiment, we decided not to pursue a rigorous deconvolution procedure. Rather, we took advantage of the fact that the RIXS map of CoO is known quite well from high-resolution measurements, and the positions of the loss peaks are well understood within simulations involving crystal-field excitations. Due to the localized character of these excitations, the RIXS signal from a single-crystal is quite similar to that from CoO nanoparticles with random orientation. Thus, even though we collect and sum the signal coming from photons scattered over a large solid angle, and consequently reduced angular resolution, the measured signal is not distorted. With this *a priori* knowledge, we simulated the RIXS spectrum as a simple sum of up to 12 Gaussian peaks, with energy positions given by those calculated in the literature (van Schooneveld *et al.*, 2012). These peaks represent the main inelastic features, and were kept fixed (on an energy-loss scale) for all incident photon wavelengths. For each measured spectrum, we calculated the best fit for the Gaussian distribution series (Igor, Wavemetrics), varying the width and amplitude of each peak and convolving them with the measured calibration spectrum of the $4f$ peaks (Fig. 2). This procedure is based on minimizing the value of χ^2 using a non-linear least-squares fitting routine *via* the Levenberg–Marquardt iterative algorithm. For all nine spectra we obtained very good fits, as depicted by the red circles for the two cases shown in Fig. 3.

The obtained RIXS map, represented on an energy-loss scale, is depicted in Fig. 4. As described earlier, at photon energies below the Co resonance peak the RIXS spectrum is dominated by the quasi-elastic line; however, at higher photon energies strong energy-loss features appear, identified earlier as $d-d$ excitations. Overall the RIXS map we measured with the PAX technique is in very good agreement with that measured through traditional grating-based spectrometers (van Schooneveld *et al.*, 2012). The width of the quasi-elastic line is ~ 0.5 eV, which is in accord with our reference Au spectrum, and represents the limit of overall resolution given the monochromatic bandwidth at the SXR instrument, the analyzer settings and the use of the $4f$ peaks of Au. It is straightforward to achieve a resolution approaching ~ 0.2 eV, limited only by the natural width of the $4f$ resonance, provided that the incident X-ray pulse is monochromated to better than this value together with using the electron analyzer in a low-pass energy operation mode, or with a narrower entrance slit.

Rigorous deconvolution is quite susceptible to noise, and can lead to non-physical (oscillatory) results (Morháč *et al.*, 1997). Therefore a regularization procedure is highly desirable. Confining the space of allowed solutions to non-negative values leads to stable iterative deconvolution procedures, the most common of these being the Gold and Richardson–Lucy algorithms (Morháč & Matoušek, 2011). The details of applying these methods to our data are beyond the scope of this work. Our recent results on this topic will be summarized in an upcoming publication.

Table 1
Comparison (per shot) between grating spectrometer and PAX.

Parameter	GS	PAX
Number of photons on the sample	2×10^{10}	2×10^{10}
Spot size (μm)	15×500	900×900
Fluence (mJ cm^{-2})	25	0.25
Fluorescence yield	10^{-3}	10^{-3}
Aluminium foil (200 nm) transmission	0.8	0.8
Collection efficiency	10^{-6}	2.5×10^{-2}
Diffraction efficiency	2.5×10^{-2}	–
Conversion to electrons	–	3×10^{-2}
Detection efficiency	0.8	0.8
Analyzer transmission	–	10^{-5}
Measured number of photons/electrons	0.15	0.05

6. Comparison with grating spectrometers and outlook

It is quite instructive to compare the performance of the PAX spectrometer with a traditional grating spectrometer (GS). Here we will use as an example the X-ray emission spectrometer developed by the Soft X-ray Department at LCLS, operating at a resolving power of ~ 2000 and equipped with a commercial CCD camera (ANDOR).

The measured performance is summarized in Table 1. This comparison is made by carrying out RIXS measurements on the same sample of CoO, mounted in a similar geometry, and by looking at the spectra accumulated at similar excitation

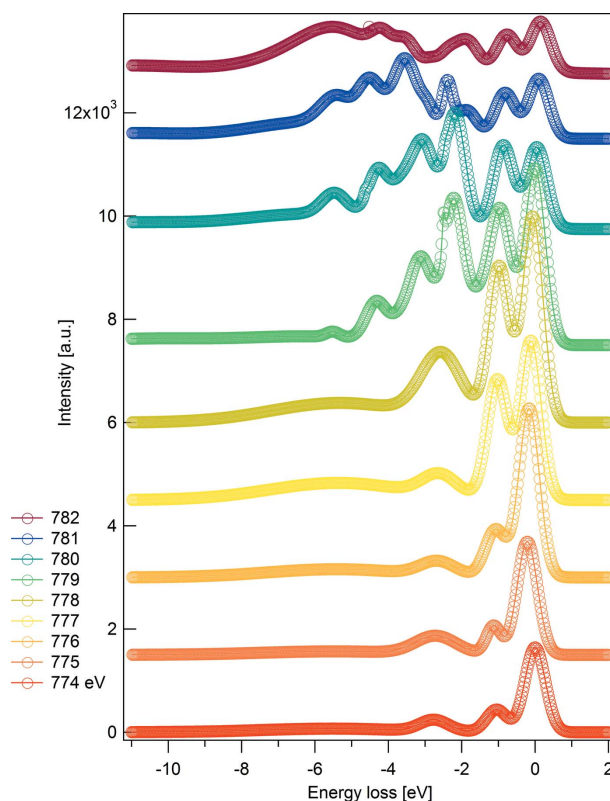


Figure 4
A RIXS map demonstrating the evolution of the inelastic spectra while scanning the incident energy across the Co edge. All the spectra shown represent a sum of (up to) 12 Gaussian functions. Upon convolution with the reference spectrum in Fig. 2, these RIXS spectra represent the best fits to the measured photoelectron spectra.

wavelengths. The incident number of photons was identical in the two measurements, and was estimated based on the transmission of the SXR beamline (Schlotter *et al.*, 2012). However, due to the difference in spot sizes the fluence on the sample was approximately 100 times higher when using the GS, which may be unacceptable for some condensed matter systems, and especially at higher repetition rates, projected for new facilities such as the X-ray FEL LCLS-II, expected in 2020. The fluorescence yield was assumed to be 0.1%, based on previous RIXS experiments (Magnuson *et al.*, 2002). The collection efficiency of the GS is based on the vertical acceptance of the grating (100 mm-long, 2° incidence angle, 800 mm from the sample) and the horizontal acceptance of the detector (6 mm-wide, 2000 mm from the sample); for PAX the collection efficiency is given only by the X-ray footprint on the converter system and the distance from the sample.

The conversion from X-rays to electrons is estimated using the partial sub-shell photoionization cross section of the 4*f* peaks in Au (Yeh & Lindau, 1985), and an inelastic mean-free path of 3 nm for the escaping photoelectrons. The analyzer transmission for the particular setting that we used was estimated to be ~0.1 mSr (Dreera *et al.*, 2014).

From this comparison it is evident that, when the total number of incident photons is the same, the PAX method already leads to a similar, slightly lower, data acquisition rate than the GS at similar total resolving power. The advantage of the PAX method becomes more significant when the two methods are scaled to the same incident fluence, where the PAX improvement reaches a factor of 30. It is also evident that the gain in collection efficiency by the PAX method is offset by the low transmission of the electron analyzer, which is known to be typically in the mSr range for hemispherical analyzers (R3000).

There are a few possibilities for significantly improving the count rate, which could lead to faster data acquisition, improved energy resolution, or both. Employing an electrostatic analyzer with a larger hemisphere radius and larger acceptance cone can improve the transmission by a factor of almost ten, for identical analyzer settings (slit and pass energy). In addition, the transmission could be improved if the photoelectrons are guided in a strong magnetic field towards the analyzer. Commercial systems have already incorporated this solution by using a specially designed magnetic immersion lens. Another option is to use a toroidal analyzer (Liu *et al.*, 2013) for even larger transmission. Thus, the overall increase in transmission can be well over a factor of 100. We conclude that PAX could become a feasible choice even at third-generation light sources and rival the performance of current GSs at moderate resolutions, as currently demonstrated.

In our test measurements, we indicated that the localized nature of the RIXS excitations in fact resulted in no significant momentum dependence of the spectra. Therefore the recorded spectra did not suffer from angular smearing. If that were not the case, an adjustable aperture could be inserted in front of the Au foil to restrict the angular acceptance, while improving the angular resolution. Alternatively, if the distance from the sample to the Au foil is significantly larger than the

X-ray footprint on the sample, every point on the Au foil would correspond to X-rays emitted from the sample at a different angle. In this case, operating the electron analyzer in the imaging mode represents an opportunity to collect RIXS maps at different transferred momenta (within a certain range) without the need to scan the sample or detector position.

Finally, the concept of implementing PAX to measure RIXS can be generalized in a straightforward way for tender and hard X-ray energies. The appeal here is that the PAX spectrometer does not rely on the use of gratings or Bragg optics, and the performance is dependent on the properties of the photoelectron spectrometer. Moreover, the inherent reduction of the sub-shell photoionization cross section at higher energies is, to a large extent, offset by the increase of the inelastic mean free path of the photoelectrons. Therefore, no significant loss is expected when converting X-ray photons to photoelectrons. With the current interest in future development of more sophisticated instrumentation needed for tender and hard X-ray photoemission spectroscopy studies, we can expect that PAX will become an appealing alternative.

In conclusion, the PAX method presented here offers significant flexibility over the traditional grating spectrometers in the soft X-ray range. Manipulating and energy-sorting photoelectrons is a much more versatile concept and it can be exploited in a variety of configurations. We are in the process of developing an improved version of the current setup that will significantly increase the signal rates and will allow us to test the ultimate resolution that can be achieved with this method.

Acknowledgements

Use of the Linac Coherent Light Source (LCLS), SLAC National Accelerator Laboratory, is supported by the US Department of Energy, Office of Science, Office of Basic Energy Sciences under Contract No. DE-AC02-76SF00515.

References

- Ament, L. J. P., van Veenendaal, M., Devereaux, T. P., Hill, J. P. & van den Brink, J. (2011). *Rev. Mod. Phys.* **83**, 705–767.
- Beye, M., Schreck, S., Sorgenfrei, F., Trabandt, C., Pontius, N., Süßler-Langeheine, C., Wurth, W. & Föhlisch, A. (2013). *Nature (London)*, **501**, 191–194.
- Chiuzbăian, S. G., Schmitt, T., Matsubara, M., Kotani, A., Ghiringhelli, G., Dallera, C., Tagliaferri, A., Braicovich, L., Scagnoli, V., Brookes, N. B., Staub, U. & Patthey, L. (2008). *Phys. Rev. B*, **78**, 245102.
- Dakovski, G. L., Heimann, P., Holmes, M., Krupin, O., Minitti, M. P., Mitra, A., Moeller, S., Rowen, M., Schlotter, W. F. & Turner, J. J. (2015). *J. Synchrotron Rad.* **22**, 498–502.
- Dell'Angela, M., Anniyev, T., Beye, M., Coffee, R., Föhlisch, A., Gladh, J., Kaya, S., Katayama, T., Krupin, O., Nilsson, A., Nordlund, D., Schlotter, W. F., Sellberg, J. A., Sorgenfrei, F., Turner, J. J., Öström, H., Ogasawara, H., Wolf, M. & Wurth, W. (2015). *Struct. Dyn.* **2**, 025101.
- Dreera, G., Salvinelli, G., Åhlund, J., Karlsson, P. G., Wannberg, B., Magnano, E., Nappini, S. & Sangaletti, L. (2014). *J. Electron Spectrosc. Relat. Phenom.* **195**, 109–116.
- Ebel, M. F. (1975). *X-ray Spectrom.* **4**, 43–46.

- Ghiringhelli, G., Piazzalunga, A., Dallera, C., Trezzi, G., Braicovich, L., Schmitt, T., Strocov, V. N., Betemps, R., Patthey, L., Wang, X. & Griioni, M. (2006). *Rev. Sci. Instrum.* **77**, 113108.
- Heimann, P., Krupin, O., Schlotter, W. F., Turner, J., Krzywinski, J., Sorgenfrei, F., Messerschmidt, M., Bernstein, D., Chalupský, J., Hájková, V., Hau-Riege, S., Holmes, M., Juha, L., Kelez, N., Lüning, J., Nordlund, D., Fernandez Perea, M., Scherz, A., Soufli, R., Wurth, W. & Rowen, M. (2011). *Rev. Sci. Instrum.* **82**, 093104.
- Hennies, F., Pietzsch, A., Berglund, M., Föhlisch, A., Schmitt, T., Strocov, V., Karlsson, H. O., Andersson, J. & Rubensson, J.-E. (2010). *Phys. Rev. Lett.* **104**, 193002.
- Irwin, K. & Hilton, G. (2005). *Cryogenic Particle Detection*, edited by C. Enss, Vol. 99 of *Topics in Applied Physics*, pp. 63–149. Berlin: Springer-Verlag.
- Krause, M. O. (1965). *Phys. Rev.* **140**, A1845–A1849.
- Liu, X.-J., Nicolas, C. & Miron, C. (2013). *Rev. Sci. Instrum.* **84**, 033105.
- Long, J. P., Itchkawitz, B. S. & Kabler, M. N. (1996). *J. Opt. Soc. Am. B*, **13**, 201–208.
- Magnuson, M., Butorin, S. M., Guo, J.-H. & Nordgren, J. (2002). *Phys. Rev. B*, **65**, 205106.
- Mårtensson, N., Baltzer, P., Brühwiler, P. A., Forsell, J.-O., Nilsson, A., Stenborg, A. & Wannberg, B. (1994). *J. Electron Spectrosc. Relat. Phenom.* **70**, 117–128.
- Morháč, M., Kliman, J., Matoušek, V., Veselský, M. & Turzo, I. (1997). *Nucl. Instrum. Methods Phys. Res. A*, **401**, 385–408.
- Morháč, M. & Matoušek, V. (2011). *J. Comput. Appl. Math.* **235**, 1629–1640.
- Nordgren, J. & Guo, J. (2000). *J. Electron Spectrosc. Relat. Phenom.* **110–111**, 1–13.
- Nordgren, J. & Rubensson, J.-E. (2013). *J. Electron Spectrosc. Relat. Phenom.* **188**, 3–9.
- Schlotter, W. F., Turner, J. J., Rowen, M., Heimann, P., Holmes, M., Krupin, O., Messerschmidt, M., Moeller, S., Krzywinski, J., Soufli, R., Fernández-Perea, M., Kelez, N., Lee, S., Coffee, R., Hays, G., Beye, M., Gerken, N., Sorgenfrei, F., Hau-Riege, S., Juha, L., Chalupsky, J., Hajkova, V., Mancuso, A. P., Singer, A., Yefanov, O., Vartanyants, I. A., Cadenazzi, G., Abbey, B., Nugent, K. A., Sinn, H., Lüning, J., Schaffert, S., Eisebitt, S., Lee, W.-S., Scherz, A., Nilsson, A. R. & Wurth, W. (2012). *Rev. Sci. Instrum.* **83**, 043107.
- Schooneveld, M. M. van, Kurian, R., Juhin, A., Zhou, K., Schlappa, J., Strocov, V. N., Schmitt, T. & de Groot, F. M. F. (2012). *J. Phys. Chem. C*, **116**, 15218–15230.
- Soman, M. R., Hall, D. J., Tutt, J. H., Murray, N. J., Holland, A. D., Schmitt, T., Raabe, J. & Schmitt, B. (2013). *J. Instrum.* **8**, C01046.
- Takata, Y., Yabashi, M., Tamasaku, K., Nishino, Y., Miwa, D., Ishikawa, T., Ikenaga, E., Horiba, K., Shin, S., Arita, M., Shimada, K., Namatame, H., Taniguchi, M., Nohira, H., Hattori, T., Södergren, S., Wannberg, B. & Kobayashi, K. (2005). *Nucl. Instrum. Methods Phys. Res. A*, **547**, 50–55.
- Tiedtke, K., Sorokin, A. A., Jastrow, U., Juranić, P., Kreis, S., Gerken, N., Richter, M., ARP, U., Feng, Y., Nordlund, D., Soufli, R., Fernández-Perea, M., Juha, L., Heimann, P., Nagler, B., Lee, H. J., Mack, S., Cammarata, M., Krupin, O., Messerschmidt, M., Holmes, M., Rowen, M., Schlotter, W., Moeller, S. & Turner, J. J. (2014). *Opt. Express*, **22**, 21214–21226.
- Uhlig, J., Doriese, W. B., Fowler, J. W., Swetz, D. S., Jaye, C., Fischer, D. A., Reintsema, C. D., Bennett, D. A., Vale, L. R., Mandal, U., O’Neil, G. C., Miaja-Avila, L., Joe, Y. I., El Nahhas, A., Fullagar, W., Parnefjord Gustafsson, F., Sundström, V., Kurunthu, D., Hilton, G. C., Schmidt, D. R. & Ullom, J. N. (2015). *J. Synchrotron Rad.* **22**, 766–775.
- Wernet, P., Kunnus, K., Josefsson, I., Rajkovic, I., Quevedo, W., Beye, M., Schreck, S., Grübel, S., Scholz, M., Nordlund, D., Zhang, W., Hartsock, R. W., Schlotter, W. F., Turner, J. J., Kennedy, B., Hennies, F., de Groot, F. M. F., Gaffney, K. J., Techert, S., Odelius, M. & Föhlisch, A. (2015). *Nature (London)*, **520**, 78–81.
- Yeh, J. & Lindau, I. (1985). *At. Data Nucl. Data Tables*, **32**, 1–155.